A X-Band Capacitor-Coupled QVCO Using Sinusoidal Current Bias Technique

I-Shing Shen and Christina F. Jou

***Abstract*—This study introduces an X-band quadrature voltage-controlled oscillator (QVCO) based on two novel techniques: capacitor coupling and sinusoidal current biasing. The proposed QVCO achieves an excellent figure-of-merit (FOM) of 190.5 dBc/Hz. This study analyzes the properties of this QVCO, including its phase noise, oscillation frequency, and amplitude. To generate quadrature phase signals with low phase noise, the proposed design uses two capacitor-coupled LC-tank cores instead of active device—coupled cores. Sinusoidal currents through these capacitors bias the oscillator, increasing oscillation amplitude and reducing the phase noise contribution from cross-coupled transistors compared to existing QVCOs or VCOs biased with a constant current. These two techniques allow the proposed QVCO to achieve at least a theoretical 3 dB phase noise improvement compared to conventional LC-QVCOs. Implemented in a standard 0.18 μm CMOS process, the proposed QVCO had a frequency tuning range of 9.2$\sim$10.4 GHz and a phase noise of -115.7 dBc/Hz@1 MHz from a carrier of 10.4 GHz while consuming 3.6 mW with 1.5 V voltage supply.**

***Index Terms*—Quadrature voltage-controlled oscillator (QVCO), sinusoidal bias technique, capacitor-coupled, phase noise, oscillation amplitude.**

I. Introduction

QUADRATURE signals are typically used in many receiver and transmitter architectures as local oscillators (LOs), generating up- and down-conversions with image-reject mixing. A widely-used approach for generating a quadrature signal is to couple two identical LC-voltage-controlled-oscillators (LC-VCOs) biased with constant current sources (dc current sources). The parallel-QVCO (P-QVCO) proposed by Rofougaran *et al.* [1], reproduced in Fig. 1(a), is a well-known implementation of this principle. This design couples two standard LC-VCOs biased with constant current of $I_{\rm bias}$ through the additional coupling transistors $Qc_1 \sim Qc_8$ in parallel with the cross-coupled transistors. However, the P-QVCO suffers from a trade-off between phase noise and phase accuracy [2]. The coupling transistors in the P-QVCO limit the tuning range of the oscillation frequency and degrade the phase noise, oscillation amplitude, and the quality of the LC-tank. More details of the P-QVCO and the standard VCO are in [4] and [3], respectively. To avoid the undesired effects of the coupling transistors in the P-QVCO and relax the trade-off between phase noise and phase accuracy, researchers have proposed two popular topologies: the series-QVCO (S-QVCO) and back-gate-QVCO (BG-QVCO) proposed in [5] and [6], respectively. The S-QVCO is a cascade configuration in which the coupling transistors are connected in series with cross-coupled transistors and the BG-QVCO couples the signals through the back-gate terminals of the cross-coupled transistors. However, the coupling transistors in the S-QVCO must be much larger than the cross-coupled transistors for minimum phase noise contribution, which overloads the resonator and hence limits the operating frequency and frequency tuning range [7]. The BG-QVCO also suffers from the overloading because the large signals coupled at the back gate may forward bias the substrate junction.

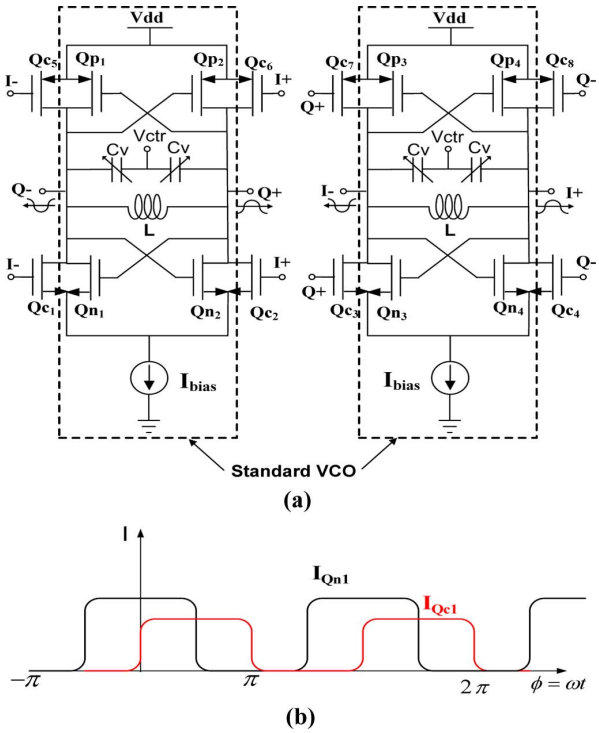

Fig. 1. (a) Conventional P-QVCO consisted of two standard VCOs and coupling transistors. (b) Drain current waveforms of Qn1 and Qc1.

The current shaping technique also can be employed to reduce the phase noise contributed by cross-coupled transistors [8]. This technique adds the second harmonic current to the constant bias current, which modulates the noise power of the cross-coupled transistors and in turn reduces the phase noise. However, in practical implementations, the added second harmonic current is asymmetrical due to parasitic capacitors, which

Manuscript received May 10, 2011; revised October 13, 2011; accepted October 21, 2011. Date of publication January 09, 2012; date of current version February 03, 2012.

The authors are with the Department of Communication Engineering, National Chiao Tung University, Hsinchu 30010, Taiwan (e-mail: yistaropip@msn.com; christ@cc.nctu.edu.tw).

Color versions of one or more of the figures in this paper are available online at http://ieeexplore.ieee.org.

Digital Object Identifier 10.1109/TMTT.2011.2176957

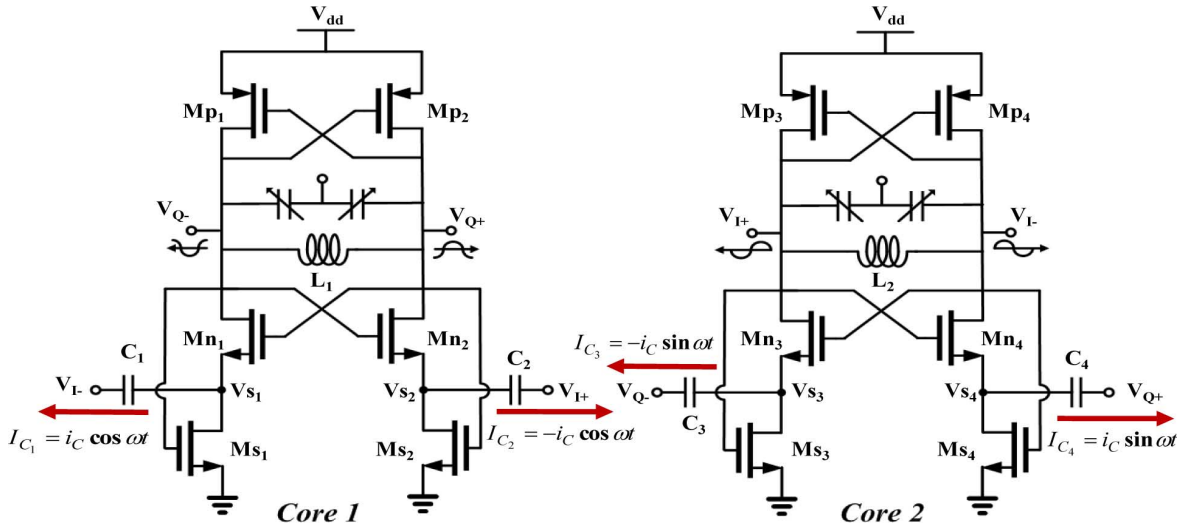

Fig. 2. Schematic of the proposed CC-QVCO biased with the sinusoidal currents of $Ic_1 \sim Ic_4$.

prevents the oscillator from achieving the expected phase noise improvement [8], [9].

This study proposes a capacitor-coupled QVCO (CC-QVCO) biased with sinusoidal current. The CC-QVCO adopts two novel techniques: 1) using capacitor to couple two LC-tank cores for quadrature generation and 2) employing sinusoidal currents through these coupling capacitors to bias the oscillator. The analysis and comparisons presented in this paper show that the CC-QVCO removes the undesirable effects caused by the coupling transistors in the P-QVCO, increases the oscillation amplitude, and reduces phase noise contributed by cross-coupled transistors. Compared to the P-QVCO, the CC-QVCO can achieve a theoretical 3 dB phase noise improvement, as verified by simulations. The CC-QVCO was implemented in a 0.18 um CMOS process and achieved a low phase noise of -115.7 dBc/Hz at 1 MHz offset from the X-band frequency of 10.3 GHz while consuming 3.6 mW with 1.5 V supply. For the state of the art, the CC-QVCO achieves an excellent figure of Merit (FoM) of 190.5, which even outperforms some lower-frequency oscillators.

This paper is organized as follows. Section II presents the CC-QVCO design, describing the large-signal operation model and the sinusoidal current waveform bias technique. This section also analyzes the oscillation amplitude and oscillation frequency. Section III describes the phase noise analysis for the constant current and sinusoidal current bias techniques and compares the phase noise simulations of the CC-QVCO with VCO, BG-QVCO, and S-QVCO. Section IV presents the measurement results. Finally, Section V presents conclusions.

II. Capacitor-Coupled QVCO (CC-QVCO) Biased With Sinusoidal Current

Before introducing the proposed topology, this section reviews the conventional P-QVCO of Fig. 1(a). An important design parameter in the P-QVCO is coupling strength S, which is defined as the ratio of the gate-width of the coupling transistor W_{Qc} to the gate-width of the cross-coupled transistor W_{Qn}, i.e., $S = W_{Qc1}/W_{Qn1}$ [4]. In practical implementation

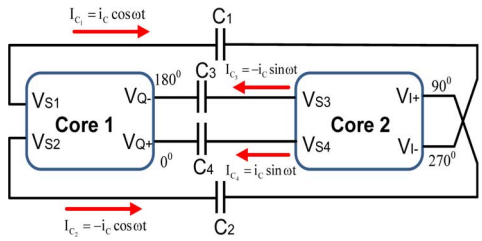

Fig. 3. Block schematic and signal phases for proposed QVCO.

of the P-QVCO, the coupling strength is usually between $1/3 \sim 1/2 (1/3 < S < 1/2.)$. The dc current, I_{bias}, serves as the current source for biasing two LC-tank cores. Assuming all transistors in the P-QVCO act like ideal switches in the large-signal condition and the oscillator operates in current-limited regime, two cross-coupled NMOS transistors in each core, including Qn_1 and Qn_2, alternatively turn on to steer the part of I_{bias}. At the same time, the coupling NMOS transistors, such as Qc_1 and Qc_2, alternatively turn on to steer the remaining part of I_{bias}. Therefore, I_{Qc1} and I_{Qn1} can be modeled as square waveforms as depicted in Fig. 1(b).

Fig. 2 shows a schematic of the proposed capacitor-coupled QVCO (CC-QVCO), in which two identical LC-tank cores, Core1 and Core2, are coupled passively by coupling capacitors $C_1 \sim C_4$ instead of actively coupled by coupling transistors as in conventional *LC*-QVCOs [1], [5], [6]. In each core, the complementary structure is employed using both PMOS and NMOS transistors in cross-coupled pair as negative resistance to compensate for the losses of the LC-tank. The self-switch transistors, $Ms_1 \sim Ms_4$, can be automatically switched on and off by injecting output signals V_{I-}, V_{I+}, V_{Q+} and V_{Q-} back into their gates. Similar to conventional LC-QVCOs using the active devices connection, the CC-QVCO using passive capacitor connection also can be modeled as a ring structure with quadrature phase signals as shown in Fig. 3. The CC-QVCO's steady-state output voltage signals can be approximated as $V_{Q+} = A_t \cos \omega t, V_{Q-} = -A_t \cos \omega t, V_{I+} = A_t \sin \omega t$ and

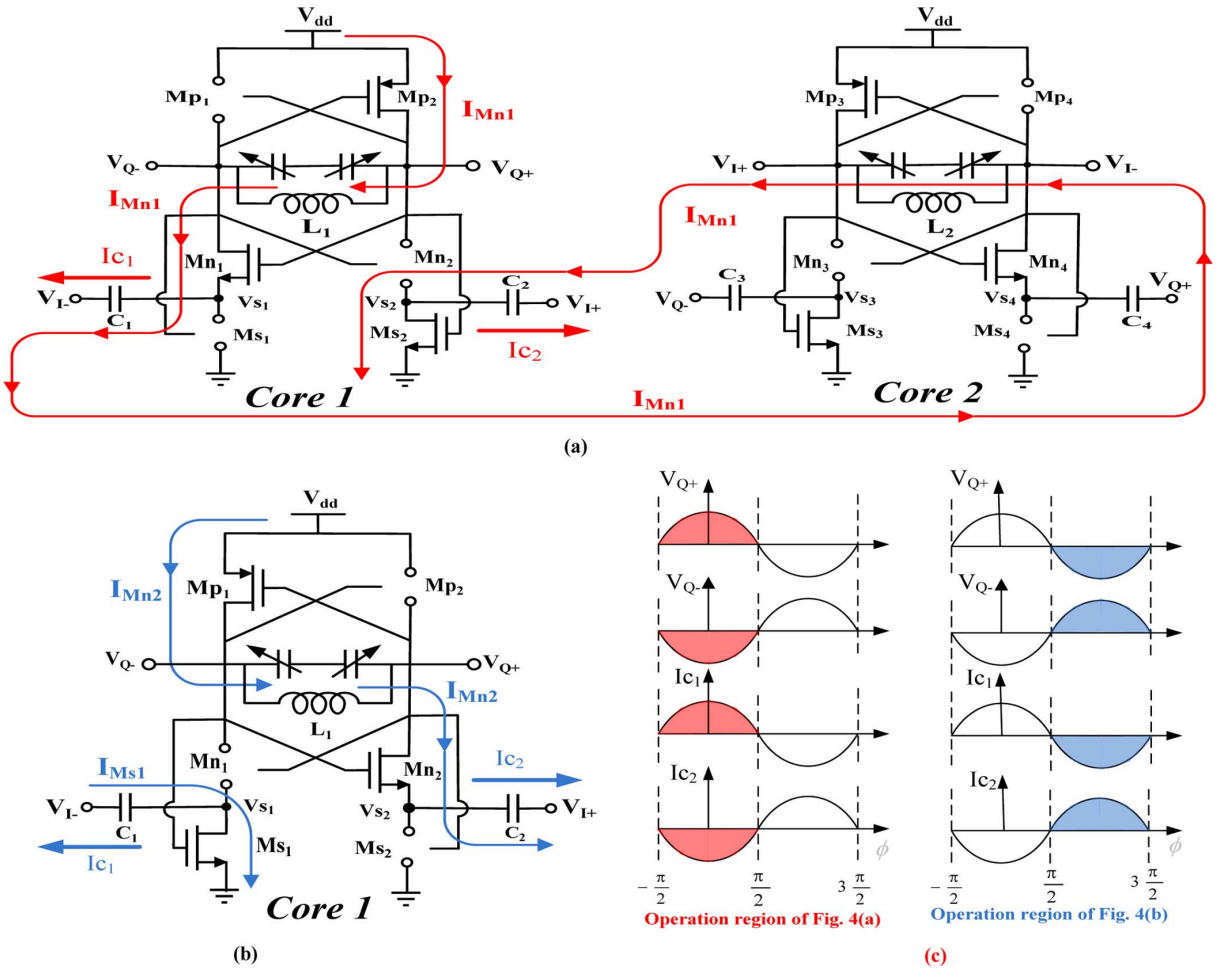

Fig. 4. (a) Completely current path of the CC- QVCO during the positive half cycle of $V_{Q+}(-\pi/2 \leq \phi \leq \pi/2)$. (b) Operation mechanism of core 1 during the negative half cycle of $V_{Q+}(\pi/2 \leq \phi \leq \pi 3/2)$ (c) Presented waveforms of V_{Q+}, V_{Q-}, Ic_1 and Ic_2 during the positive and negative half cycle of V_{Q+}.

$V_{I-} = -A_t \sin \omega t$, where A_t is the single-ended amplitude and ω is the oscillation frequency.

Because the self-switched transistors $Ms_1 \sim Ms_4$ operate in the triode region, their ac drain-source voltages, $Vs_1 \sim Vs_4$, are much smaller than the output voltage signals. We can assume that the ac voltages across the coupling capacitors are almost equal to the associated output voltage signals (i.e., $Vs_1 - V_{I-} \approx -V_{I-} = A_t \sin \omega t$). Thus, currents through coupling capacitors, denoted as Ic_1, Ic_2, Ic_3 and Ic_4 in Fig. 2, present the sinusoidal waveforms dominated by the associated output signals. For example, Ic_1, which passes from Vs_1 to V_{I-}, can be approximately expressed as

$$Ic_1 \approx C_1 \frac{d}{dt} A_t \sin(\omega t) = C_1 A_t \omega \cos(\omega t) = i_C \cos(\phi) \tag{1}$$

where i_C, defined as the amplitude of Ic_1, is the product of $A_t C_1$, and ω, and the angle $0 \leq \phi \leq 2\pi$ is used instead of ωt. Using the same approach, the currents of C_2, C_3 and C_4 can be respectively written as $I_{C2} = -i_c \cos \omega t, I_{C3} = -i_c \sin \omega t$ and $I_{C4} = i_c \sin \omega t$. Note that the directions of $Ic_1 \sim Ic_4$ are all defined as to be from the drains of self-switched transistors to the associated output signals (i.e., the direction of Ic_1 is defined as from Vs_1 to V_{I+}.). As long as the oscillation amplitudes are sufficiently large, the sinusoidal currents passing through the coupling capacitors can serve as current sources to properly bias the oscillator. Assuming that all transistors in the CC-QVCO act like ideal switches, the cross-coupled NMOS and PMOS transistors are perfectly complementary and the CC-QVCO operates in current limit region, Fig. 4(a) and (b) illustrate the operation of this bias technique in a large signal condition. The shadow regions of V_{Q+}, V_{Q-}, Ic_1 and Ic_2 shown in Fig. 4(c) denote the presented waveforms when the CC-QVCO operates at the positive and negative half cycle of V_{Q+}. Observe Core1 in Fig. 4(a): at the positive half cycle of $V_{Q+}(-\pi/2 \leq \phi \leq \pi/2)$, when Ms_1 and Mp_1 turn off, Mn_1 and Mp_2 turn on to steer the positive half cycle of Ic_1 from V_{dd} to Vs_1. However, during the cycle $(-\pi/2 \leq \phi \leq \pi/2)$, a potential problem in the CC-QVCO is how the drain current of Mn_1, I_{Mn1}, can be steered to the ground from Vs_1. Based on the defined directions of Ic_1 and Ic_2 in Fig. 2 and referring to Fig. 4(a), the sinusoidal current, Ic_2, is in its negative half cycle (note Ic_2 is in phase with Ic_1.) and steered to the ground by Ms_2. This means $I_{Mn1} = I_{Ms2} = i_C \cos \phi$ during the cycle of $-\pi/2 \leq \phi \leq \pi/2$. Therefore, the complete drain current path of I_{Mn1} is from V_{dd} to the ground by flowing through the LC-tank of the Core2 as shown in Fig. 4(a). On the contrary, to

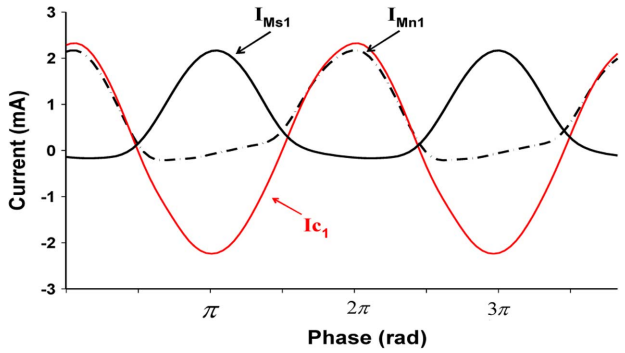

Fig. 5. Simulated current waveforms of I_{Mn1}, I_{Ms1} and I_{C1} in the current limit region.

see Fig. 4(b), at the negative cycle of $V_{Q+}(\pi/2 \le \phi \le \pi 3/2)$, Mn_1 and Mp_2 are off while Ms_1 is on. Since the polarity of Ic_1 reverses during this period, the negative half of Ic_1 can be steered to the ground by Ms_1, which means $I_{Ms1} = -i_C \cos\phi$ during the cycle of $\pi/2 \le \phi \le \pi 3/2$. Fig. 5 shows the simulated waveform of I_{Mn1}, I_{Ms1} and Ic_1. As can be seen in Fig. 5, the positive half of Ic_1 is equal to I_{Mn1} and the negative half of Ic_1 is in phase with I_{Ms1}, confirming the large-signal operation described in Fig. 4(a) and (b). In summary, in each half cycle of V_{Q+}, Mn_1 and Ms_1 steers the sinusoidal current Ic_1, and hence, the drain current of $Mn_1(Mp_2)$ and of Ms_1, $I_{Mn1}(I_{Mp2})$ and I_{Ms1}, is shaped as the positive half of Ic_1 and negative half of Ic_1, respectively.

Based on this large-signal operation mechanism of the CC-QVCO, the drain currents I_{Mn1}, I_{Mp2} and I_{Ms2} during a period of $-\pi \le \phi \le \pi$ can be expressed as

$$I_{Mn1} = I_{Mp2} = I_{Ms2} = \begin{cases} i_C \cos\phi, & -\pi/2 \le \phi \le \pi/2 \\ 0, & \text{otherwise.} \end{cases} \tag{2}$$

Because of the symmetry of the oscillator, the drain currents I_{Mn2}, I_{Mp1} and I_{Ms1} during a period of $-\pi \le \phi \le \pi$ can be written as

$$I_{Mn2} = I_{Mp1} = I_{Ms1} = \begin{cases} -i_C \cos\phi, & \text{otherwise} \\ 0, & -\pi/2 \le \phi \le \pi/2. \end{cases} \tag{3}$$

Using the Fourier expression for the positive half of sinusoidal current waveform with the amplitude of i_C given in Appendix I, the Fourier expression for I_{Mn1} can be expressed as

$$I_{Mn1} = \frac{i_C}{\pi} + \frac{i_C}{2}\cos\phi + \sum_{n=2,4,6\ldots}^{\infty} \left(\frac{2i_C}{\pi}\right)\left(\frac{2n}{1-n^2}\right)\cos n\phi. \tag{4}$$

From (4), the DC component, I_0, and the magnitude of the first harmonic, I_1, of the drain current of Mn_1 are $I_0 = i_C/\pi$ and $I_1 = i_C/2$, respectively. Based on (2), (3) and (4), all drain currents of transistors in the CC-QVCO have the same dc component I_0 and the magnitude of the first harmonic current I_1. The total dc current consumption per core is $2I_0$.

The above property of the CC-QVCO in the large signal condition shows that the sinusoidal current bias technique strongly depends on the interaction between the two cores; this interaction makes the two cores operate as two current generators for biasing each other. For instance, to see Fig. 3, by coupling capacitor C_2, a quadrature phase voltage $V_{I+} = A_t \sin\omega t$ in Core2 is translated to an in-phase current $I_{C1} = i_C \cos\omega t$ and then this current injects into Vs_2 as a bias current of Core1. Moreover, note that the CC-QVCO is incapable of oscillation without coupling capacitors. Because transistor Mn_1 and Ms_1 alternatively turns on, the coupling capacitors C_1 are required for injecting its sinusoidal currents to drive Mn_1 and Ms_1 and guarantee oscillation startup. In the other words, a core of the CC-QVCO cannot oscillate alone. This is unlike the conventional OVCO topologies [1], [6] that can become two LC-VCOs after removing their coupling components (i.e., the P-QVCO of Fig. 1(a) can become two standard LC-VCOs after removing $Qc_1 \sim Qc_8$.).

The following section analyzes the oscillation frequency for the CC-QVCO. Based on Fig. 2, the equivalent circuit of LC-tank Core1, including the coupling path, is depicted in Fig. 6(a), in which R_P is the equivalent parallel resistor of LC-tank Core1, C_P is the parasitic capacitance at output nodes and $Rs_4(Rs_3)$ is the input resistance looking into node $Vs_4(Vs_3)$ of Core2 from $C_4(C_3)$. Fig. 6(a) also depicts the harmonic currents and injected quadrature current. The currents having the form of $I_1\cos\phi$ are the first harmonic currents of the drain currents of the cross-coupled transistors in Core1 and $i_C \sin\phi$ are the injected quadrature current through coupling capacitors C_3 and C_4 from Core2. Considering g_m as the small signal transconductance of Mn_4 and $R_{\rm on}$ as the drain-to-source resistance of Ms_4, the input resistance Rs_4 can be written as $Rs_4 = R_{\rm on}//(1/g_m)$. The resistance $Rs_4(Rs_3)$ is actually quite small because $Ms_4(Ms_3)$ operating in the triode region leads to a small resistance $R_{\rm on}$. On the other hand, for the CC-QVCO, the coupling capacitances $C_1 \sim C_4$ must be as small as possible for minimum phase noise, as described in the next section. Assuming that the impedance of $C_4(C_3)$ is sufficiently larger than $Rs_4(Rs_3)$, for the series of $1/sC_1$ and Rs_4, Rs_4 can be ignored. Thus, the equivalent circuit of LC-tank Core1 shown in Fig. 6(a) can be simplified as an equivalent resonator as shown in Fig. 6(b), where the equivalent resonator in Fig. 6(b) consists of C_v, C_p, L_1, C_4, C_3 and R_p,. To observe Fig. 6(b), the oscillation frequency, ω_o, can be easily obtained by

$$\omega_0 = \frac{1}{\sqrt{L(C_V + C_P + C_C).}} \tag{5}$$

Note that this oscillation frequency of the CC-QVCO is a resonant frequency, which is unlike that oscillation frequencies of the conventional LC-QVCOs are away from resonance. For example, the LC-tank of the P-QVCO must introduce a phase shift to maintain loop gain at unity since the first harmonic current injecting into LC-tank from the coupling transistors is quadrature to that from the cross-coupled transistors. According to [10], this phase shift causes the equivalent circuit of the LC-tank in the P-QVCO to operate away from its own resonant frequency, reducing the effective Q of the resonator and hence

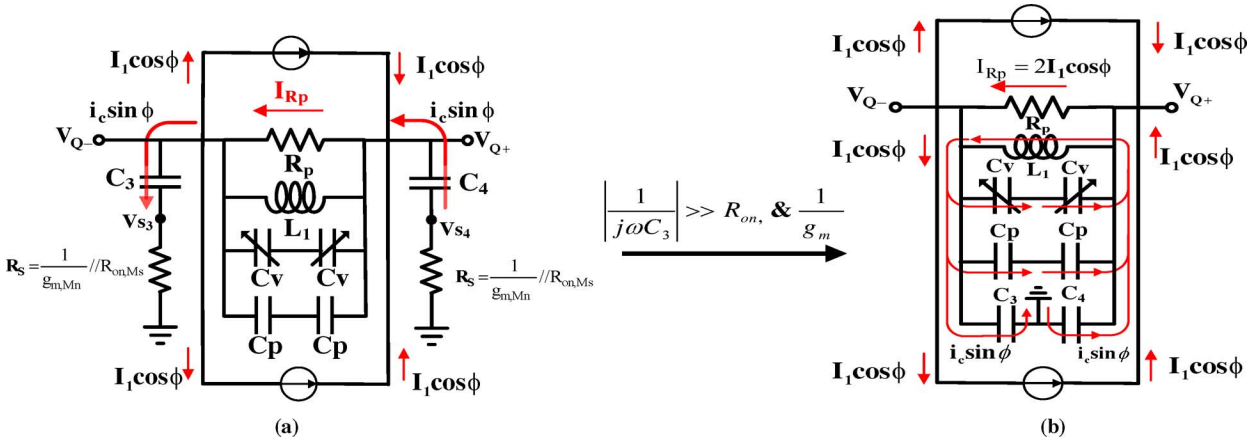

Fig. 6. (a) Equivalent circuit of LC-tank Core1 with harmonic currents and quadrature injected current. (b) Simplified equivalent circuit as the impedance of C_1 is much larger than $R_{\rm on}$ and $1/g_m$.

degrading the phase noise. However, by using passive components $C_1 \sim C_4$, the equivalent circuit of LC-tank in the CC-QVCO does not need to introduce a phase shift. It is because, as shown in Fig. 6(b), injected quadrature current through C_3 and C_4, $i_C \sin\phi$, can be considered as the currents inside the equivalent resonator operating at the resonant frequency. The property of no required phase shift ensures that the oscillator operates at a resonant frequency, and obtains maximum effective Q. This property helps achieve the excellent phase noise performance in QVCO implementations.

Next, this study derives the oscillation amplitude of the CC-QVCO. For comparison, we set the dc current consumption per core in the CC-QVCO equal to a standard VCO of Fig. 1(a) so that $I_{\rm bias} = 2I_0$. Through $I_0 = i_C/\pi$ in (4), the amplitude of the sinusoidal current of coupling capacitor, i_C, can be set at

$$i_c = \frac{\pi}{2} I_{\rm bias}. \tag{6}$$

From Fig. 6(b), the current through Rp, I_{Rp}, is $I_{Rp} = 2I_1 \cos\phi$ and hence through $I_1 = i_C/2$ in (4), the differential oscillation amplitude, A, can be calculated as the product of i_C and R_p

$$A = i_c R_p = \frac{\pi}{2} I_{\rm bias} R_p. \tag{7}$$

For a given dc current consumption per core of $I_{\rm bias} = 2I_0$ and an effective parallel resistance of R_p, the standard VCO biased with a constant current of $I_{\rm bias}$ has an oscillation amplitude of $4I_{\rm bias}R_p/\pi$ [11], while the CC-QVCO achieves an oscillation amplitude of $\pi I_{\rm bias}R_p/2$, which is 23% larger than the VCO. However, according to [4], the amplitude of the P-QVCO falls sharply as the coupling strength S increases. The practical amplitude degradation is more than 25% when the coupling strength is $S = 1/2$, where the degradation is defined as the ratio of P-QVCO oscillation amplitude to VCO. Therefore, with the same dc current consumption per core, the CC-QVCO biased with sinusoidal current can be expected to have a least 23% larger amplitude than the P-QVCO biased with constant current. Fig. 7 shows the simulated single-ended output waveform for the standard VCO, the P-QVCO with $S = 1/2$ and the CC-QVCO, showing that the actual amplitude improvement for the standard VCO and for the P-QVCO is about 19% and 38%,

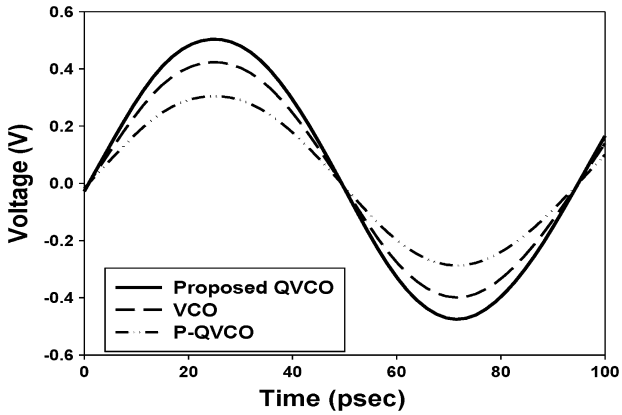

Fig. 7. Simulated output waveforms for CC-QVCO, VCO and P-QVCO with $S = 1/2$ under the same dc current consumption per core of 1 mA and the same LC-tank.

respectively. These results confirm that compared to the conventional bias topology of using constant current, using sinusoidal current to bias the oscillator is more efficient in translating dc power to oscillation signal.

III. Phase Noise Analysis

This section analyzes the phase noise for the CC-QVCO and compares it with the phase noise of the QVCOs using other topologies. The phase noise is caused by the noise current from the components in an oscillator. According to Hajimiri's impulse sensitivity function (ISF) theory [13], in an oscillator, the total single-sideband phase noise at the offset frequency $\Delta\omega$ from carrier is given by [13], [14]

$$L(\Delta\omega) = 10\log\left[\frac{\sum N_{L,i}}{2A_t^2 C_T^2 (\Delta\omega)^2}\right] \tag{8}$$

with A_t is the oscillation amplitude across the resonator, C_T is the tank capacitance, and $N_{L,i}$ is the effective noise contributed by the ith noise source. When a noise source is cyclostationary, its noise current power density, $\overline{i}^2_{n,i}(\phi)/\Delta f$ can be expressed as

$$\frac{\overline{i}^2_{n,i}(\phi)}{\Delta f} = i'^2_{n,i}\alpha_i^2(\phi) \tag{9}$$

where $i'^2_{n,i}$, the stationary noise power, is defined as the peak value of $\overline{i^2_{n,i}}(\phi)/\Delta f$ and $\alpha_i(\phi)$ is the noise modulation function (NMF) that is a periodic unit-less function with a peak value of unity [15]. Using information presented in (9), the effective noise, $N_{L,i}$, can be obtained as [14]

$$N_{L,i} = i'^2_{n,i}\frac{1}{2\pi}\int_{-\pi}^{\pi}\Gamma_i^2(\phi)\alpha_i^2(\phi)d\phi \tag{10}$$

$$= i'^2_{n,i}\frac{1}{2\pi}\int_{-\pi}^{\pi}\Gamma^2_{i,\text{eff}}(\phi)d\phi \tag{11}$$

$$= i'^2_{n,i}\Gamma^2_{i,\text{eff},RMS} \tag{12}$$

where the ISF, denoted as $\Gamma_i(\phi)$ in (10), represents the time-varying sensitivity of the oscillator's phase to perturbation, the effective ISF, denoted as $\Gamma_{i,\text{eff}}(\phi)$ in (11), is defined as $\Gamma_{i,\text{eff}}(\phi) = \Gamma_i(\phi)\alpha_i(\phi)$, and $\Gamma_{i,\text{eff}\cdot RMS}(\phi)$ is the root-mean-square (RMS) value of $\Gamma_{i,\text{eff}}(\phi)$.

According to [4], most of the effective noise in an oscillator is contributed by transistors directly connected to the LC-tank (such as Qn_1, Qc_1 and Mn_1). Hence, this study focuses on deriving the effective noise from these transistors in the CC-QVCO and in the P-QVCO. To keep equations simple, a signal-end analysis based on the approach described in [8] is performed in this study.

A. Phase Noise for Constant Current Biasing P-QVCO

It is well known that in the P-QVCO, the coupling transistors not only degrade the oscillation amplitude but also contribute additional effective noise, resulting in poor phase noise. The P-QVCO can achieve its best phase noise performance when it has no coupling transistors. In the case of the P-QVCO with no coupling transistors ($S = 0$), the P-QVCO degenerates to become as the two standard VCOs. Thus, the effective noise is only introduced by its cross-coupled transistors.

This section reviews the analysis of phase noise for a standard VCO and the associated results revealed in [8] to predict the phase noise performance of the P-QVCO. For a standard VCO biased with constant current of I_{bias}, the cross-coupled transistors Qn_1 and Qn_2 alternatively steer the constant current of I_{bias}. As a result, the thermal noise of Qn_1 (Qn_2) exhibits noise-cyclestationary property. The thermal noise of Qn_1 is $\overline{i^2_{n,Qn1}}(\phi)/\Delta f = 4kT\gamma g_{m,Qn1}$ when Qn_1 is conducting current ($-\pi/2 \le \phi \le \pi/2$), and it is close to zero when Qn_1 is off. Note that $g_{m\cdot Qn1} = \sqrt{2\beta_{Qn1}I_{\text{BIAS}}}$ is the transconductance of Qn_1 when conducting and operating in saturation with the drain current of I_{bias} and β_{Qn1} is the current gain of Qn_1. Based on the above noise property and referring to (9), $\overline{i^2_{n,Qn11}}(\phi)/\Delta f$ during an oscillation period of $-\pi \le \phi \le \pi$ can be expressed as

$$\frac{\overline{i^2_{n,Qn1}}}{\Delta f}(\phi) = i'^2_{n,Qn1}\alpha^2_{Qn1}(\phi) = \begin{cases} 4kT\gamma\sqrt{2\beta_{Qn1}I_{\text{bias}}}, & -\pi/2 \le \phi \le -\pi/2 \\ 0, & \text{otherwise} \end{cases} \tag{13}$$

where $i'^2_{n,Qn1} = 4kT\gamma\sqrt{2\beta_{Qn1}I_{\text{bias}}}$ is the stationary noise power of $\overline{i^2_{n,Qn1}}(\phi)/\Delta f$ and $\alpha_{Qn1}(\phi)$ is a (0,1) square waveform as

$$\alpha_{Qn1}(\phi) = \begin{cases} 1, & -\pi/2 \le \phi \le \pi/2 \\ 0, & \text{otherwise.} \end{cases} \tag{14}$$

The effective ISF of Qn_1 is defined as $\Gamma_{\text{eff},Qn1} = \Gamma_{Qn1}(\phi)\alpha_{Qn1}(\phi)$; $\Gamma_{Qn1} = \sin(\phi)$ is an approximation of the ISF associated with Qn_1 [8], [16], and it is easy to obtain that $\Gamma^2_{Qn1,\text{eff},RMS} = 0.25$ [8]. Substituting $i'^2_{n,Qn1}$ and $\Gamma^2_{Qn1,\text{eff},RMS}$ into (12), the effective noise of Qn1 in a stand-alone standard VCO with bias current of I_{bias} can be given by

$$N_{L,Qn1} = 4kT\gamma\sqrt{2\beta I_{\text{bias}}}(0.25). \tag{15}$$

It can be expected that the overall effective noise contributed by a pair of Qn_1 and Qc_1 in the P-QVCO, $N_{L,Qn1} + N_{L,Qc1}$, is larger than (15) due to the additional noise contribution from Qc_1.

B. Phase Noise for Sinusoidal Current Biasing CC-QVCO

On contrary to the transistors, the capacitors are noiseless. Using coupling capacitors $C_1 \sim C_4$ in the CC-QVCO instead of the coupling transistors $Qc_1 \sim Qc_8$ in the P-QVCO for quadrature signal generation can promotes phase noise performance. It is because all effective noise contributions from $Qc_1 \sim Qc_8$ in the P-QVCO such as $N_{L,Qc1}$ can be removed. The sinusoidal current biasing technique can also reduce the effective noise contribution from cross-coupled transistors, further improving phase noise. The following discussion proves this reduction by deriving the effective noise of Mn_1 in the CC- QVCO.

Considering $g_{m,Mn1}(\phi)$ as the transconductance of the cross-coupled transistor Mn_1, the noise current power density of Mn_1 is $\overline{i^2_{n,Mn1}}/\Delta f = 4kT\gamma g_{m\cdot Mn1}(\phi)$ when Mn_1 is conducting current. Assume that the CC-QVCO has the same dc current consumption as the P-QVCO. Thus, based on (2) and (6) for substitution into $g_{m,Mn1}(\phi) = \sqrt{2\beta_{Mn1}I_{d,Mn1}(\phi)}, \overline{i^2_{n,Mn1}}(\phi)/\Delta f$ during an oscillation period of $-\pi \le \phi \le \pi$ can be expressed as

$$\begin{aligned} &\frac{\overline{i^2_{n,Mn1}}}{\Delta f}(\phi) \\ &= i'^2_{n,Mn1}\alpha^2_{Mn1}(\phi) \\ &= 4kT\gamma g_{m,Mn1}(\phi) \\ &= 4kT\gamma\sqrt{2\beta_{Mn1}I_{d,Mn1}(\phi)} \\ &= \begin{cases} 4kT\gamma\sqrt{\pi\beta_{Mn1}I_{\text{bias}}\cos\phi}, & -\pi/2 \le \varphi \le -\pi/2 \\ 0, & \text{otherwise} \end{cases} \end{aligned} \tag{16}$$

where $i'^2_{n,Mn1} = 4kT\gamma\sqrt{\pi\beta I_{\text{bias}}}$ is the stationary noise power of $\overline{i^2_{n,Mn1}}(\phi)/\Delta f$. During the transistor conducting cycle of $-\pi/2 \le \phi \le \pi/2, \overline{i^2_{n,Mn1}}(\phi)/\Delta f$ in the CC-QVCO presents a time-varying form, which is unlike in the standard VCO biased with constant $I_{\text{bias}}, \overline{i^2_{n,Qn11}}(\phi)/\Delta f$ is constant. This time-varying form of noise power in the CC-QVCO is due to the term

of $(\cos\phi)^{1/2}$ introduced by the sinusoidal bias technique. To observe (16), the NMF of Mn_1, $\alpha_{Mn1}(\phi)$, now is to become the product of a (0,1) square waveform and $(\cos\phi)^{1/4}$, i.e.,

$$\alpha_{Mn1}(\phi) = \begin{cases} (\cos\phi)^{\frac{1}{4}}, & (-\pi/2 \le \phi \le \pi/2) \\ 0, & (\text{otherwise}). \end{cases} \quad (17)$$

Given $\Gamma_{Mn1} = \sin(\phi)$, the effective ISF associated with Mn_1 is defined as $\Gamma_{\text{eff},Mn1} = \sin(\phi)\alpha_{Mn1}(\phi)$. Substituting $i'^2_{n,Mn1} = 4kT\gamma\sqrt{\pi\beta I_{\text{bias}}}$ and $\Gamma_{\text{eff},Mn1}(\phi)$ into (12) makes it possible to calculate the amount of effective noise contributed by Mn_1, $N_{L,Mn1}$, i.e.,

$$\begin{aligned} N_{L,Mn1} &= i'^2_{n,Mn1}\Gamma^2_{\text{eff},Mn1,RMS} \\ &= 4kT\gamma\sqrt{\pi\beta I_{\text{bias}}}\left(\frac{1}{2\pi}\int_{-\pi/2}^{\pi/2}\sin^2(\phi)\sqrt{\cos\phi}d\phi\right) \\ &\approx 4kT\gamma\sqrt{\pi\beta I_{\text{bias}}}(0.156) \quad (18) \\ &= 4kT\gamma\sqrt{2\beta I_{\text{bias}}}(0.196) \quad (19) \end{aligned}$$

where the value denoted in (18), 0.156, is $\Gamma^2_{Mn1,\text{eff},RMS}$. Assuming $\beta_{Qn1} = \beta_{Mn1}$, comparing (15) with (19) shows that $N_{L,Mn1}$ in the CC-QVCO is even 20% smaller than $N_{L,Qn1}$ in a stand-alone standard VCO, resulting in a 1 dB phase noise improvement.

The reason for the effective noise of (19) smaller than (15) is that the cross-coupled transistor in an oscillator biased with sinusoidal current achieves a smaller $\Gamma^2_{\text{eff},RMS}$ compared to that biased with constant current. For Mn_1 in sinusoidal current biasing CC-QVCO and Qn_1 in constant current biasing VCO, $\Gamma^2_{Mn1,\text{eff},RMS} = 0.156$ is 38% smaller than $\Gamma^2_{Qn1,\text{eff},RMS} = 0.25$, which translates to a smaller effective noise contribution from Mn_1 in the CC-QVCO. Fig. 8(a) presents the simulated the NMFs and ISFs for both cross-coupled transistors Qn_1 in a standard VCO and Mn_1 in the CC-QVCO, providing an intuitive understanding of the expected reduction of $\Gamma^2_{\text{eff},RMS}$. A comparison of NMF of Mn_1 with NMF of Qn_1 shows that Mn_1 exhibits a better property of noise-cyclostationary than Qn_1. It can be seen in Fig. 8(a) that the NMF of Mn_1 is lower than NMF of Qn_1, especially when the oscillator is quite sensitive. Moreover, the NMF of Mn_1 is close to zero when the oscillators are at the maximum sensitivity points that are the maximum magnitude of the ISFs as indicated at t_1 and t_2 of Fig. 8(a). Therefore, based on $\Gamma_{i,\text{eff}}(\phi) = \Gamma_i(\phi)\alpha_i(\phi)$, we can expect that compared to the NMF of Qn_1, the NMF of Mn_1 can result in a smaller square RMS value of the effective ISF ($\Gamma^2_{Mn1,\text{eff},RMS} \le \Gamma^2_{Qn1\cdot\text{eff}\cdot RMS}$). Fig. 8(b) shows simulated effective ISFs associated with Qn_1 and Mn_1. The simulated $\Gamma^2_{Mn1,\text{eff},RMS}$ is about 31% smaller than $\Gamma^2_{Qn1,\text{eff},RMS}$. This reduction reduces the effective noise of cross-coupled transistor, improving phase noise. Although the arguments and simulations above are limited to noise-property of Qn_1 in a standard VCO, they are equally applicable to the noise-properties of the cross-coupled transistors in the QVCOs using constant current bias topology (such as P-QVCO and BG-QVCO.).

C. Design Consideration for Coupling Capacitance of the CC-QVCO

The above phase noise analysis for QVCOs is based on the assumption that the noise current from a transistor translates itself to phase noise only on its own LC-tank core rather than on both cores. This is generally valid for coupling the two LC-tank cores that operate independently, such as the P-QVCO. However, since the operation of the CC-QVCO depends strongly on the interaction between the two LC-tank cores, the phase noise contributions from the neighboring core must also be considered. The noise currents from a neighboring core inject into the LC-tank through coupling capacitors, reducing phase noise performance of the CC-QVCO. Fig. 9(a) illustrates this effect on the phase noise of the CC-QVCO, in which the noise current generated by Ms_1 (Mn_4) of Core1 (Core2), denoted as $i_{n,Ms1}$ ($i_{n,Mn4}$), is partially injected into the LC-tank of Core2 (Core1) by flowing through coupling capacitor $C_1(C_4)$. The amount of the noise current through C_1 is determined by the ratio of the coupling capacitance to parasitic capacitance C_P at the node $Vs_1(Vs_4)$. If C_1 (C_4) is much smaller than C_P (i.e., C_1 has higher impedance than C_p), almost all noise current $i_{n,Ms1}(i_{n,Mn4})$ enters C_p to the ground. Thus, for Core2 (Core1), the injecting noise current from Core1 (Core2) can be greatly reduced to improve phase noise. Therefore, the coupling capacitance $C_1 \sim C_4$ should be as small as possible to reduce the phase noise contributed by a neighboring core.

Unfortunately, when the impedances of $C_1 \sim C_4$ are excessively high, the oscillator suffers from the failure of the sinusoidal bias technique because the interaction dominating this bias technique becomes too weak, and its phase noise thus worsens. In the condition of excessive high impedances of $C_1 \sim C_4$, the coupling path connecting the two cores, such as

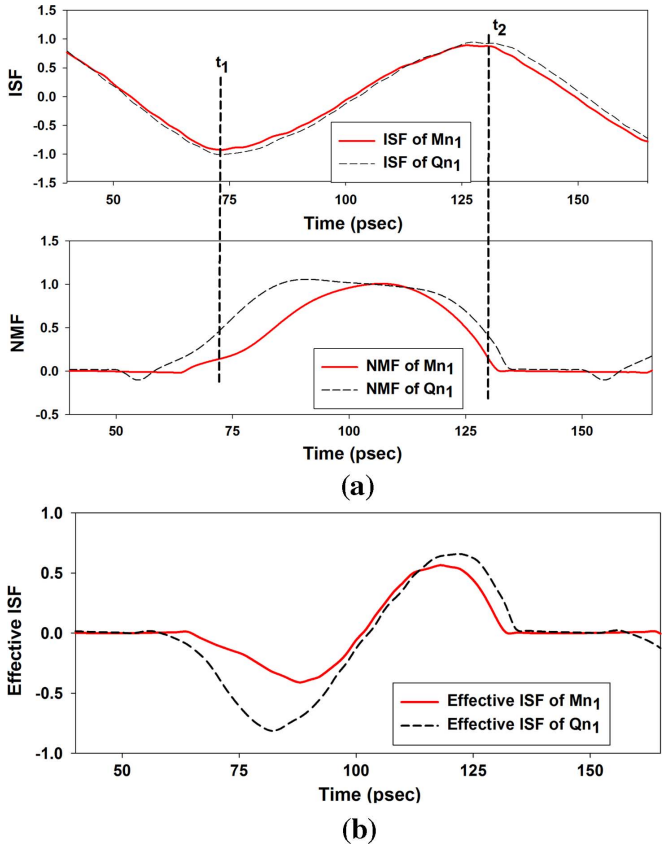

Fig. 8. (a) Simulated ISFs and NMFs for Qn_1 in the standard VCO and Mn_1 in the CC-QVCO. (b) Simulated effective ISFs of Qn_1 and Mn_1.

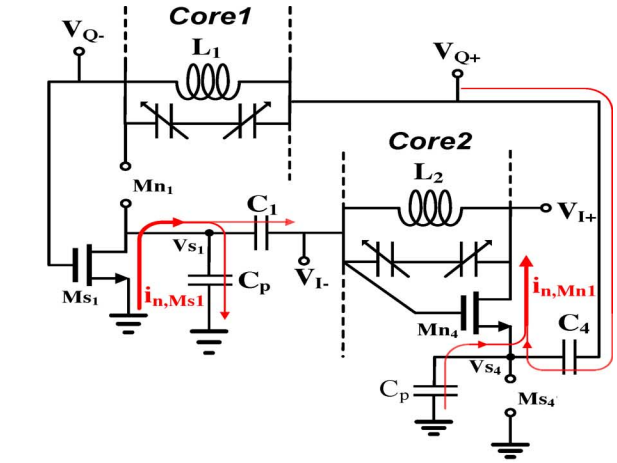

(a)

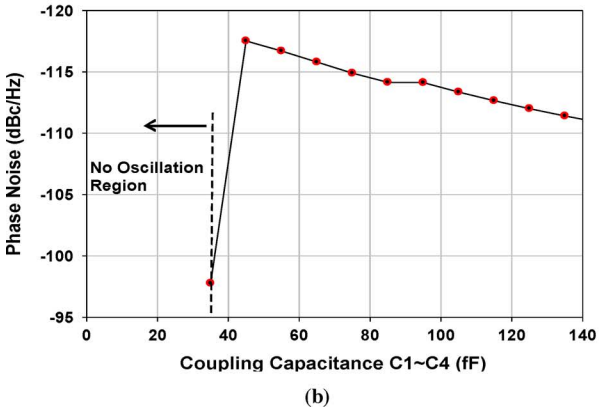

(b)

Fig. 9. (a) Effect of the interaction on phase noise of CC-QVCO. (b) Simulated phase noise of CC-QVCO at 1 MHz offset under varied coupling capacitance $C_1 \sim C_4$.

the path from Vs_1 to V_{I+}, can almost be considered as an open circuit. It is because the injected currents $Ic_1 \sim Ic_4$ that server as current sources for the CC-QVCO are too small to generate enough oscillation amplitudes to switch off transistors. In the other words, the operation of the CC-QVCO is no longer in the large signal condition. Therefore, the two cores operate independently and cannot properly bias each other through $C_1 \sim C_4$. Fig. 9(b) shows the phase noise of the CC-QVCO versus coupling capacitance $C_1 \sim C_4$. In Fig. 9(b), the phase noise is improved by reducing coupling capacitance $C_1 \sim C_4$. However the CC-QVCO's phase noise suddenly degrades due to the failure of the sinusoidal bias techniques when $C_1 \sim C_4$ are less than about 50 pF. As $C_1 \sim C_4$ drop to less than 35 fF, the CC-QVCO even enters a no oscillation region. To simultaneously avoid phase noise contribution from a neighbor core and ensure that the sinusoidal biasing technique can be implemented successfully, an appropriate coupling capacitance $C_1 \sim C_4$ can be carefully chosen by the simulation results of Fig. 9(b). The proposed design uses a value of approximately 65 fF.

In conclusion, based on (8), the phase noise can be improved by 1) increasing the oscillation amplitude, and 2) reducing effective noise associated with the noise source. With the same current consumption per core, the oscillation amplitude and the

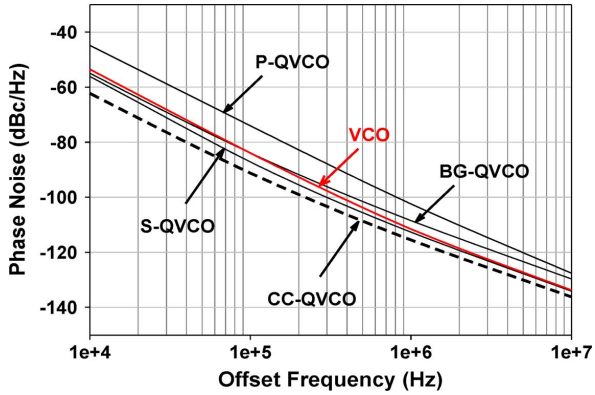

Fig. 10. Simulated phase noise of P-QVCO, S-QVCO, BG-QVCO, VCO and proposed CC-QVCO, where all oscillators operate at 10 GHz and has the same dc current consumption per core.

effective noise contributions from the cross-coupled transistors in the CC-QVCO is respectively 23% larger and 20% smaller than for the standard VCO. Assuming that $C_1 \sim C_4$ have sufficiently high impedances to ignore the noise current from the neighbor core, the phase noise of the CC-QVCO is theoretically 3 dB lower than the standard VCO. This 3 dB improvement consists of 2 dB from an oscillation amplitude increase of 23% and about 1 dB from a 20% reduction of effective noise associated with the cross-coupled transistor. Because the coupling transistor $Qc_1 \sim Qc_8$ in the P-QVCO contributes the additional effective noise and degrades oscillation amplitude, the phase noise performance of P-QVCO with $S > 0$ is worse than that of a standard VCO with the half power consumption of the P-QVCO. Therefore, compared to a P-QVCO with $S > 0$, the CC-QVCO can achieves at least a 3 dB phase noise improvement.

D. Phase Noise Simulations and Comparisons

Fig. 10 compares the simulated phase noise of the CC-QVCO with the BG-QVCO, the S-QVCO, the P-QVCO, and the standard VCO. The standard VCO was built as a P-QVCO with no coupling transistors. In all simulations, the oscillators used the same sizes of the complementary cross-coupled structures and the same inductors. Capacitances were adjusted as necessary to make the oscillation frequencies close to 10 GHz. An ideal constant current source was supplied to bias the VCO and each core of BG-QVCO, the S-QVCO, and the P-QVCO. This constant current source was identical to the dc current per core of the CC- QVCO so that in all oscillators the power consumptions per core remained the same at a supply voltage of 1.5 V. To fairly compare the performance of QVCOs, the phase noise should be compared only when all QVCOs have the same level of phase error [7]. Therefore, by adjusting back-gate coupling path of the BG-QVCO and coupling transistor's size in the S-QVCO and P-QVCO, the phase errors of all QVCOs were less than 1°.

Fig. 10 shows that the P-QVCO exhibited the worst phase noise performance due to its smallest oscillation amplitude and the additional phase noise contribution from the coupling transistors. The phase noise performance of the BG-QVCO and the S-QVCO were much better than that of the P-QVCO, and they were quite close to that of the standard VCO. By biasing the

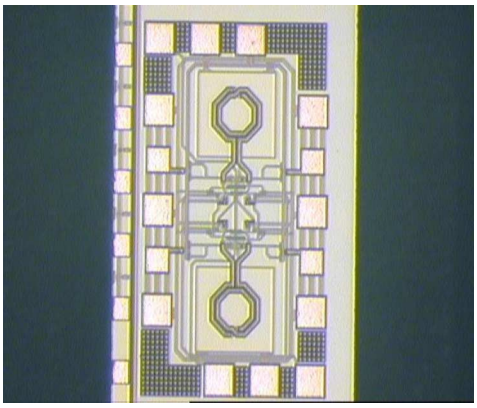

Fig. 11. Chip photograph of the fabricated CC-QVCO.

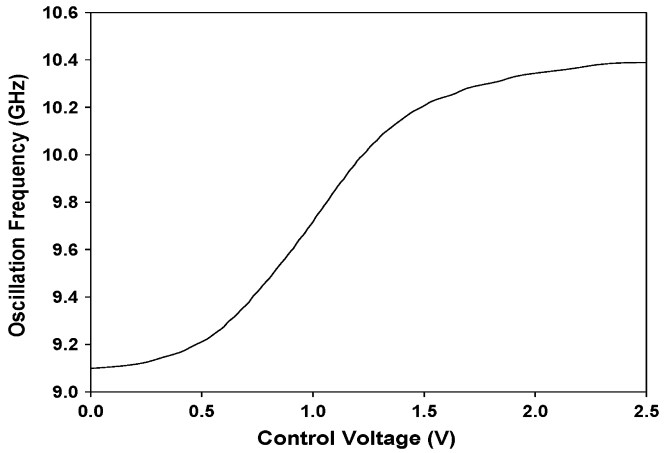

Fig. 12. Measured tunnig range of the CC-QVCO.

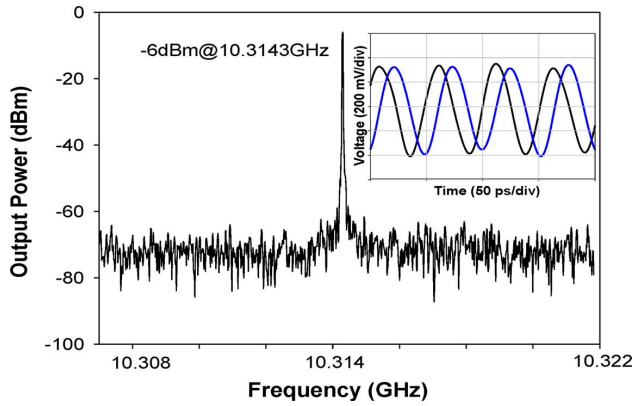

Fig. 13. Measured frequency spectrum of the CC-QVCO and time domain output waveform at 10.314 GHz.

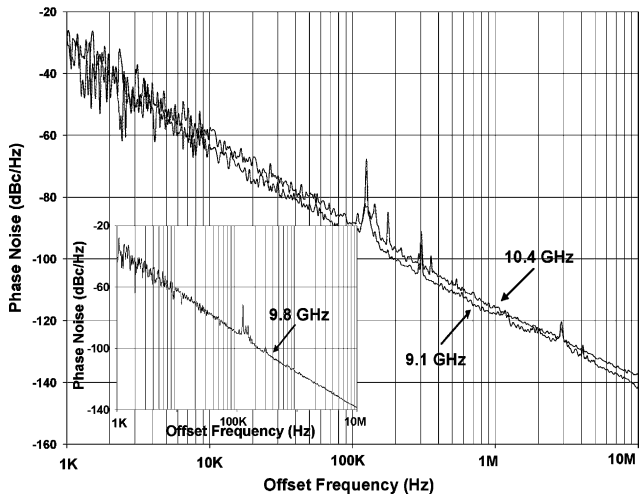

Fig. 14. Measured phase noise of the CC-QVCO oscillating at 10.4, 9.1 and 9.8 GHz under the voltage supply of 1.5 V.

oscillator in the sinusoidal current to increase oscillation amplitude and reduce the effective noise associated with cross-coupled transistors, the CC-QVCO exhibited the best phase noise performance. Compared to the standard VCO, the CC-QVCO presented a 2.5 dB phase noise improvement at 1 MHz offset, which agrees well with the theoretical expectations of a 3 dB phase noise improvement. Compared to the P-QVCO, the practical phase noise improvement is about 11.5 dB, where the coupling strength S of the P-QVCO is $S = 1/2$.

IV. Measurement

A capacitor-coupled QVCO biased with sinusoidal current (CC-QVCO) was fabricated in TSMC 0.18 μm mixed-signal/RF CMOS 1P6M technology. Fig. 11 shows a microphotograph of the fabricated CC-QVCO with its source-follower buffers. The chip area, including all pads, is 0.7×1.1 mm^2. We used the bias-tees to connect the buffers as a load while doing measurement. To verify that quadrautre signals can be captured on an oscilloscope, any mismatch in the length of measurement cables has been calibrated out.

The CC-QVCO core draw 2.4 mA and consumed a dc power of only 3.6 mW under a 1.5 V voltage supply. Fig. 12 shows the measured CC-QVCO frequency tuning range. The oscillation frequency increased from 9.1 GHz to 10.4 GHz when the controlled voltage increased from 0 to 2.5 V, corresponding to a frequency tuning range of 10.3%. Fig. 13 shows the single-ended output spectrum and real-time quadrature output waveform when the CC-QVCO oscillates at 10.3 GHz. The measured output power is -6 dBm and phase error is about 1.5°. Fig. 14 shows the plots of phase noise as the CC-QVCO operated at maximum, minimum and central frequency. The phase noise at 1 MHz offset was -115.7 dBc/Hz, -117.4 dBc/Hz and -116.2 dBc/Hz, measured at 10.4 GHz, 9.1 GHz, and 9.8 GHz carrier frequency, respectively. The phase noise at offset frequency between 100 KHz to 10 MHz shows the trend of 1/f^2 and it is dominated by the thermal noise of components in the circuit. The CC-QVCO achieved superior FOM of 190.5 as operating at 10.4 GHz, where FOM is defined as [17]

$$\text{FoM} = -L(\Delta f) + 20\log\left(\frac{f_o}{\Delta f}\right) - 10\log\left(\frac{P_{dc}}{1\,mW}\right). \quad (20)$$

Table I summarizes the performance of the CC-QVCO and presents the results from previously published QVCOs and VCOs.

V. Conclusion

This study analyzes two novel techniques, capacitor-coupling and sinusoidal current biasing of the oscillator, and successfully fabricates a 0.18 um COMS X-band QVCO. The pro-

TABLE I
PERFORMANCE SUMMARY AND COMPARISON

Ref.	Technology	Frequency (GHz)	Topology	Diff. /Quad.	Phase Noise @1MHz (dBc/Hz)	Power (mW)	Tuning Rang (%)	FOM (dBc/Hz
[7]	0.18-um CMOS	17	Transformer Coupled	Quad.	-110	5	17	188
[18]	0.25-um CMOS	5	Superharmonic Coupling	Quad.	-124	22	10	185
[19]	0.13-um CMOS	10.0	Cascode-based coupling	Quad.	-95	14.4	15	163
[20]	0.18-um CMOS	9.6	phase-tunable injection-coupled	Quad.	-121@3MHz	9	6.6.	182.6
[21]	0.18-um CMOS	2.2	Self Switched Biasing	Quad.	-134	36	18	185
[22]	90-um CMOS	10.0	Cross-Coupled	Diff.	-109.2	7.5	15.8	180
[23]	0.18-um CMOS	5.6	Capacitive feedback	Diff.	-118	3	6.4	189
[24]	PCB	9.5	Tunable SIW Resonator	Diff.	-117	37	7	184
This Work	**0.18-um CMOS**	**10.4**	**Proposed QVCO**	**Quad.**	**-115.7**	**3.6**	**10**	**190.5**

posed capacitor-coupling QVCO biased with sinusoidal current (CC-QVCO) is a topology choice for a high-performance quadrature signal generator. This study also discusses the advantages of the sinusoidal current bias technique over a conventional oscillator biased with constant current, including oscillation amplitude and the phase noise contribution from cross-coupled transistors. Using passive devices, coupling capacitors, instead of active-devices for quadrature generation introduces no increase in phase noise.

The proposed CC-QVCO achieved a low phase noise of 115.7 dBc/Hz at 1 MHz offset from the carrier of 10.4 GHz while consuming only 3.6 mW. The CC-QVCO occupies a core area of 0.77 mm^2. The excellent FOM of 191 of this design confirms its validity and advantages.

APPENDIX

If $f(t)$ is a positive half of sinusoidal waveform with period of T and amplitude of i_C, it can be written as

$$f(t) = i_C \cos\left(\frac{2\pi t}{T}\right) \sum \prod \left(\frac{2\pi t/T - 2k\pi}{\pi}\right) \tag{21}$$

where $\prod(x)$ is a single pulse centered at the origin with unity amplitude and defined as

$$\prod(x) = \begin{cases} 1, & -0.5 \le x \le 0.5 \\ 0, & \text{otherwise.} \end{cases} \tag{22}$$

Then, the Fourier series expansion for $f(t)$ is

$$f(t) = b_0 + b_1 \cos\left(\frac{2\pi t}{T}\right) + \sum_{n=2\ldots}^{\infty} b_n \cos\left(\frac{2\pi n t}{T}\right) \tag{23}$$

where

$$b_0 = \frac{1}{T} \int_{-T/2}^{T/2} f(t)\, dt = \frac{i_C}{\pi} \tag{24}$$

$$b_1 = \frac{2}{T} \int_{-T/2}^{T/2} f(t) \cos\left(\frac{2\pi t}{T}\right) dt = \frac{i_C}{2} \tag{25}$$

$$\begin{aligned} b_n &= \frac{2}{T} \int_{-T/2}^{T/2} f(t) \cos\left(\frac{2n\pi t}{T}\right) dt \\ &= \frac{2}{T} \int_{-T/4}^{T/4} i_C \cos\left(\frac{2\pi t}{T}\right) \cos\left(\frac{2n\pi t}{T}\right) dt \\ &= \frac{i_C}{\pi} \left(\frac{2}{1-n^2}\right) \cos\left(\frac{n}{2}\pi\right). \end{aligned} \tag{26}$$

ACKNOWLEDGMENT

The authors would like to thank the National Chip Implementation Center, Hsinchu, Taiwan, for supporting chip fabrication and measurements.

REFERENCES

[1] A. Rofougaran, J. Rael, M. Rofougaran, and A. Abidi, "A 900 MHz CMOS *LC*-oscillator with quadrature outputs," in *Proc. ISSCC*, Feb. 1996, pp. 392–393.
[2] L. Romanom, S. Levantino, A. Bonfanti, C. Samori, and A. L. Lacaita, "Phase noise and accuracy in quadrature oscillators," in *Proc. IEEE Int. Symp. Circuits Syst. (ISCAS)*, 2004, vol. 1, pp. 161–164.
[3] L. Jia, J.-G. Ma, K. S. Yeo, and M. A. Do, "9.3–10.4 GHz band cross-coupled complementary oscillator with low phase-noise performance," *IEEE Trans. Microw. Theory Tech.*, vol. 52, no. 4, pp. 1273–1278, Apr. 2004.
[4] R. Aparicio and A. Hajimiri, "A noise-shifting differential colpitts VCO," *IEEE J. Solid State Circuits*, vol. 36, no. 12, pp. 1728–1736, Dec. 2002.
[5] P. Andreani, A. Bonfanti, L. Romano, and C. Samori, "Analysis and design of a 1.8-GHz CMOS *LC* quadrature VCO," *IEEE J. Solid-State Circuits*, vol. 37, no. 12, pp. 1737–1747, Dec. 2002.
[6] H.-R. Kim, C. Y. Cha, S.-M. Oh, M.-S. Yang, and S.-G. Lee, "A very low-power quadrature VCO with back-gate coupling," *IEEE J. Solid-State Circuits*, vol. 39, no. 6, pp. 952–955, Jun. 2004.
[7] A. W. L. Ng and H. C. Luong, "A 1-V 17-GHz 5-mW CMOS quadrature VCO based on transformer coupling," *IEEE J. Solid-State Circuits*, vol. 42, no. 9, pp. 1933–1941, Sep. 2007.

[8] B. Soltanian and P. R. Kinget, "Tail current-shaping to improve phase noise in *LC* voltage-controlled oscillators," *IEEE J. Solid-State Circuits*, vol. 41, no. 8, pp. 1792–1802, Aug. 2006.
[9] I. S. Shen, T. C. Huang, and C. F. Jou, "A low phase noise quadrature VCO using symmetrical tail current-shaping technique," *IEEE Microw. Wireless Compon. Lett.*, vol. 20, no. 7, pp. 399–401, Jul. 2010.
[10] B. Razavi, "A study of injection locking and pulling in oscillators," *IEEE J. Solid-State Circuits*, vol. 39, pp. 1415–1424, Sep. 2004.
[11] A. Hajimiri and T. H. Lee, "Design issues in CMOS differential *LC* oscillators," *IEEE J. Solid-State Circuits*, vol. 34, no. 5, pp. 717–724, May 2000.
[12] R. Aparicio and A. Hajimiri, "A noise-shifting differential colpitts VCO," *IEEE J. Solid-State Circuits*, vol. 36, no. 12, pp. 1728–1736, Dec. 2002.
[13] A. Hajimiri and T. H. Lee, "A general theory of phase noise in electrical oscillators," *IEEE J. Solid-State Circuits*, vol. 33, no. 2, pp. 179–194, Feb. 1998.
[14] A. Mazzanti and P. Andreani, "Class-C harmonic CMOS VCOs, with a general result on phase noise," *IEEE J. Solid-State Circuits*, vol. 43, no. 12, pp. 2716–2729, Dec. 2008.
[15] T. H. Lee and A. Hajimiri, "Oscillator phase noise: A tutorial," *IEEE J. Solid-State Circuits*, vol. 35, no. 3, pp. 326–336, Mar. 2000.
[16] P. Andreani and X. Wang, "On the phase-noise and phase-error performancesof multiphase LC CMOS VCOs," *IEEE J. Solid-State Circuits*, vol. 39, no. 11, pp. 1883–1893, Nov. 2004.
[17] P. Kinget, *Integrated GHz Voltage Controlled Oscillators*. Norwell, MA: Kluwer, 1999, pp. 355–381.
[18] S. L. J. Gierkink *et al.*, "A low-phase-noise 5-GHz COMS quadrature VCO using superharmonic coupling," *IEEE J. Solid-State Circuits*, vol. 38, pp. 1148–1154, Jul. 2005.
[19] S. Li, I. Kipnis, and M. Ismail, "A 10-GHz CMOS quadrature LC-VCO for multicore optical applications," *IEEE J. Solid-State Circuits*, vol. 38, no. 10, pp. 1626–1634, Oct. 2003.
[20] I. R. Chamas and S. Raman, "Analysis and design of a CMOS phase-tunable injection-coupled LC quadrature VCO (PTIC-QVCO)," *IEEE J. Solid-State Circuits*, vol. 44, pp. 784–796, Mar. 2003.
[21] G. Huang and B.-S. Kim, "Low phase noise self-switched biasing CMOS *LC* quadrature VCO," *IEEE Trans. Microw. Theory Tech.*, vol. 57, no. 2, pp. 344–351, Feb. 2009.
[22] K. W. Tang *et al.*, "Frequency scaling and topology comparison of mm-wave CMOS VCOs," in *Proc. IEEE CSICS*, Nov. 2006, pp. 55–58.
[23] H.-H. Hsieh and L.-H. Lu, "A high-performance CMOS voltage-controlled oscillator for ultra-low-voltage operations," *IEEE Trans. Microw. Theory Tech.*, vol. 55, no. 3, pp. 467–473, Mar. 2007.
[24] F. F. He, K. Wu, W. Hong, L. Han, and X. Chen, "A low phase-noise VCO using an electronically tunable substrate integrated waveguide resonator," *IEEE Trans. Microw. Theory Tech.*, vol. 58, no. 12, pp. 3452–3458, Dec. 2010.

I.-Shing Shen was born in Taipei, Taiwan, in 1982. He received the B.S. degree in engineering and system science from National Tsing Hua University, Hsinchu, Taiwan, in 2005, the M.S. degree in communication engineering from National Chiao Tung University (NCTU), Hsinchu, Taiwan, in 2007, and he is currently working toward the Ph.D. degree in communication engineering at the same university.

His current research is on the microwave/RF active circuit design, including mixer, LNA, VCO and QVCO.

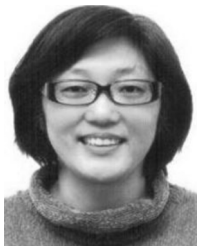

Christina F. Jou was born in Taipei, Taiwan, in 1957. She received the B.S., M.S., and Ph.D. degrees in electrical engineering from the University of California at Los Angeles (UCLA), in 1980, 1982, and 987, respectively. Her Ph.D. dissertation concerned the millimeter-wave monolithic Schottky diode-grid frequency doubler.

From 1987 to 1990, she was a member of the Technical Staff of the Microwave Products Division, Hughes Aircraft Company, Torrence, CA, where she was responsible for microwave device modeling. In 1990, she joined National Chiao Tung University, Hsinchu, Taiwan, where she is currently an Associate Professor of communication engineering. Her current research is the development of microwave/RF active circuits andmicroelectromechanical systems (MEMS) devices.